Numerical Simulation of Inertia Friction Welding Process by Finite Element Method

A model was developed to predict temperature evolution, stress, strain, and the final geometry of inertia friction welded parts

BY L. FU, L. Y. DUAN, AND S. G. DU

ABSTRACT. During friction welding, temperature, stress, strain, and their variations govern welding parameters, and knowledge of them helps determine optimum parameters and ways to improve the design and manufacture of welding machines. In the present paper, the transient temperature, stress, and strain fields in inertia welding are investigated by both numerical analytical and experimental methods. The finite element method is used for the coupled thermomechanical problem, and variable thermal properties and mechanical properties for the materials are taken into account in the analysis. The variation of temperature, deformation, stress, strain, and strain rate during inertia welding is systematically investigated and analyzed. The calculated results of temperature distribution are in good agreement with the infrared detected ones. The numerically calculated results for the shape of the welded joint also show an excellent fit with experimental observations.

Introduction

Friction welding is a complicated metallurgical process, accompanied by a series of physical phenomena: frictional heat generation, plastic deformation, cooling of high-temperature metal, and solid-state phase variation. In both the continuous-drive friction welding and inertia friction welding processes, the thermomechanical behavior at the interface is obviously critical to the quality of the welded joint.

Fiction welding is a process in which the heat for welding is produced by direct conversion of mechanical energy to thermal energy at the interface of the workpieces. In order to model the friction welding process, a combination of thermal effects and plastic deformation is needed. In 1990, Andrzej Sluzalec proposed the incremental theory for the thermal elastoplastic finite element calculation and adopted the method of the coupled thermomechanical analysis to calculate the temperature field during continuous drive friction welding (Ref. 1).

The rapid advance of computer technology has spurred commensurately rapid advancement in the numerical simulation of the complex processes frequently encountered in welding processes. Effective and accurate analytic tools are of increasing importance in welding engineering because advanced analytical capabilities can significantly reduce the lead time and cost in the design of a welding process by reducing empirical efforts required to develop proper process controls for welding products. Considerable work has been published regarding continuous-drive friction welding (Refs. 2-6). A. Moal and E. Massoni proposed in 1992 a thermomechanical model for the simulation of the inertia welding process (Refs. 7, 8). They treated the material behavior according to an incompressible viscoplastic Norton-Hoff law. The friction law was determined experimentally and depends on the prescribed pressure and the relative rotating velocity of the part. The numerical results concerning evolution of parts shape, strain, temperature, rotating velocity, and upsetting are put forward. But there is little information about the stress and the strain rate of the joint in the literature.

In this study, *DEFORM* software was used in the coupled deformation and heat flow analysis during inertia friction welding. An effort to develop a realistic model of inertia welding was undertaken. The transient temperature, stress, and strain fields for a frictional welded joint of 36CrNiMo4 steel in tubular form are calculated under given boundary conditions. Variable thermal and mechanical properties of the welded material have been taken into account. The infrared detector is used to measure the temperature distributions on the surface of the weldment and compare them with the calculated values. The observed shape of the welded joint is also compared with the calculated one.

KEY WORDS

Numerical Calculation
Inertia Welding
Temperature
Stress
Strain

L. FU, L. Y. DUAN, and S. G. DU are with Northwestern Polytechnical University, Xi'an, China.

Calculation Model

The schematic weldment for the calculation is shown in Fig. 1. The radius of its outer circle is R_2. The radius of its inner circle is R_1. The length of the workpiece is L, and the axial direction is Z-axis. Because of the rotational symmetry existing in friction welding, we only need to analyze half of the longitudinal section along Z-axis, i.e., G zone, as shown in Fig. 1. The fundamental nonsteady equation of the heat condition with changeable thermal properties in the coupled thermomechanical problem can be expressed as follows (Ref. 4):

$$\frac{1}{r}\frac{\partial}{\partial r}\left(r\lambda\frac{\partial T}{\partial r}\right)+\frac{\partial}{\partial z}\left(\lambda\frac{\partial T}{\partial z}\right)+\dot{q}=\rho c\frac{\partial T}{\partial t} \quad (1)$$

where ρ, λ, and c are the density, thermal conductivity, and specific heat of the welded material, respectively. $\dot{q}$ is the internal energy rate, the coupling factor for the thermomechanical action. It is the function of plastic work, and can be expressed as

$$\dot{q}=\beta\bar{\sigma}\dot{\bar{\varepsilon}} \quad (2)$$

where $\bar{\sigma}$ refers to equivalent stress, $\dot{\bar{\varepsilon}}$ is equivalent strain rate, and β is the thermal efficiency of plastic deformation. Here we take $\beta = 90\%$ as Ref. 4.

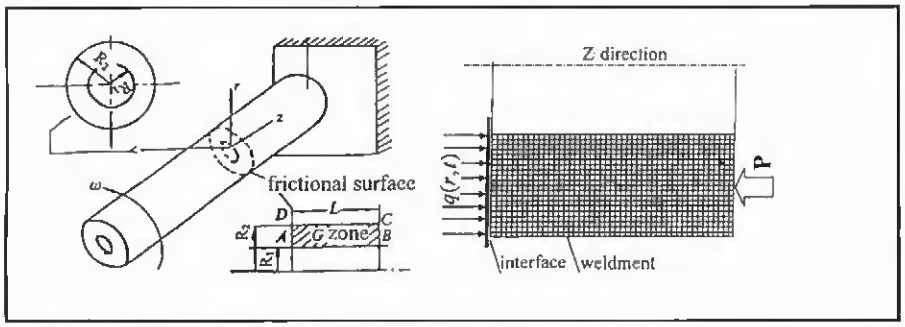

Fig. 1 — Coordinate and the zone calculated in the pipe and the boundary condition.

Table 1 — Thermal Properties of the 36CrNiMo4 Steel

Temperature (K)	200	300	573	773	973	1170	1370	1570
Thermal conductivity λ (W/m·K)	462	520	605	742	703	672	675	678
Specific heat C (J/kg·K)	43.3	42.8	40.9	37.6	31.4	32.3	34.4	35.4

Since the total welding time in the inertia process is usually very short and the contacting surfaces are not exposed to surroundings, the heat loss through convection and radiation can be neglected. Thus, the boundary condition of the temperature field can be determined as follows:

$$-k\left.\frac{\partial T}{\partial z}\right|_{z=0} = q(r,t)$$

$$\left.\frac{\partial T}{\partial r}\right|_{r=R_1,R_2} = 0$$

$$\left.\frac{\partial T}{\partial z}\right|_{z=L} = 0 \qquad (3)$$

where $q(r,t)$ refers to heat flow density at frictional surface. Inertia welding differs essentially from continuous drive friction welding by the rate of energy input. Since the rotational speed varies in inertia friction welding, the rate of heat generated at the interface due to the frictional force is a function of the distance from the center and the rotational speed.

It can be seen that the frictional coefficient depends on the thrust pressure acting on the workpiece and rubbing speed, which, in turn, vary with the r and the time. In view of the complex and correlated transient phenomena occurring at the interface during a very short period of time, an assumption is made that the product $\mu \cdot p$ is constant (Ref. 2). In addition, the experimental data indicate the speed-time history can be represented as follows:

$$n(t) = at^2 + bt + c \qquad (4)$$

By using the initial and final conditions, and one additional point selected from the actual speed curve during inertia welding, the parameters a, b, and c can be evaluated. So, the average value of the product $\mu \cdot p$ can be obtained as

$$A = \mu \cdot p = \frac{1.8IN^2}{\left(R_2 - R_1\right)^3 T\left(2aT^2 + 3bT + 6c\right)} \qquad (5)$$

where I is the polar moment of inertia of the rotating mass in lb-in.-s^2, N is the initial speed in rpm, and T is the time when $n(t) = 0$ in seconds. Thus, if the heat flow is assumed to flow equally into the stationary as well as the rotating parts, the rate of heat input going into both parts is linearly proportional to r at a given instant and can be expressed by

$$q = 3.6 \times 10^{-4} \cdot A \cdot r \cdot n(t) \quad kW/m^2 \qquad (6)$$

where μ is the coefficient of friction, p is the unit thrust pressure MPa, r is the distance from the center m, $n(t)$ is the rotating speed rpm, which is a function of time.

The thermal properties (thermal conductivity, specific heat) vs. temperature used in the calculation are given in Table 1, which is matched by spline interpolation function.

Kirchhoff's balance equation or its equivalent virtual work equation is still adopted for the stress and strain analysis during the inertia welding

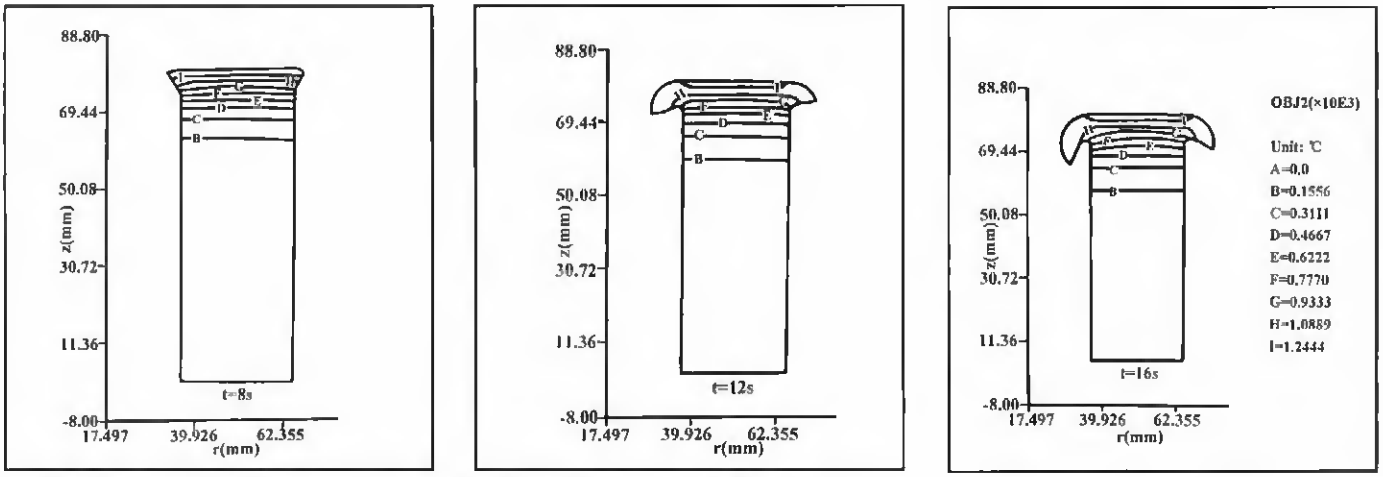

Fig. 2 — The isotherm distribution in a quarter section of the joint with time of welding.

$$\int_{V_0} S_{IJ}\delta E_{IJ}dV = \int_{V_0} P_{Oi}\delta u_i dV + \int_{S_o} T_{Oi}\delta u_i ds \quad (7)$$

where S_{IJ} is Kirchhoff's stress tensor, δE_{IJ} is Green's strain tensor, δu_i is the component of virtual displacement, and P_{Oi} and T_{Oi} are, respectively, components of body force and surface traction acting on the deformed body. Moreover, for the inertia friction welding process, the above equation for a solid subject should combine thermal and mechanical loads.

If the large deformation thermal elastoplastic problem is treated as a rheologic process, the constitutive Equation 7 can be deduced by means of the increment constitutive equation of small deformation thermal elastoplastic, that is

$$\left\{\sigma_{ij}^{\nabla}\right\} = \left[D\right]_{ep}\left(\left\{D_{ij}\right\} - \left\{D_{ij}^{\theta}\right\}\right) + \left\{\dot{\sigma}_{\theta}\right\} \quad (8)$$

where

$$\left\{D_{ij}^{\theta}\right\} = \left(\left\{a\right\} + \frac{d\left[D\right]_e^{-1}}{dT}\left\{\sigma\right\}\right)\dot{T}$$

(for initial strain rate)

$$\left\{\dot{\sigma}_{\theta}\right\} = \frac{\left[D\right]_e \frac{\partial\bar{\sigma}}{\partial\left\{\sigma\right\}}\frac{\partial H}{\partial T}\dot{T}}{H_T' + \left\{\frac{\partial\bar{\sigma}}{\partial\left\{\sigma\right\}}\right\}^T\left[D\right]_e\frac{\partial\bar{\sigma}}{\partial\left\{\sigma\right\}}}$$

$[D]_{ep}$ = elastoplastic matrix
(for initial stress rate)

In the present paper, the following boundary condition for calculation has been adopted as shown in Fig. 1. The fixed end of the workpiece is adopted as the force boundary condition (BC line). The frictional surface of the workpiece is supposed to have zero displacement condition (AD line). The outer and inner surfaces can be regarded as a free displacement condition. Besides, surface force is applied to the nodes of the finite element mesh in order to simulate mechanical loading. These forces exist in those nodes at the plane of contact between two elements, which are welded. If a node moves out from the contact plane during the process, the value of applied force is equal to zero.

To solve the equations stated above, we present finite element equations for the problem to be analyzed. They are Equations 9 and 10, respectively.

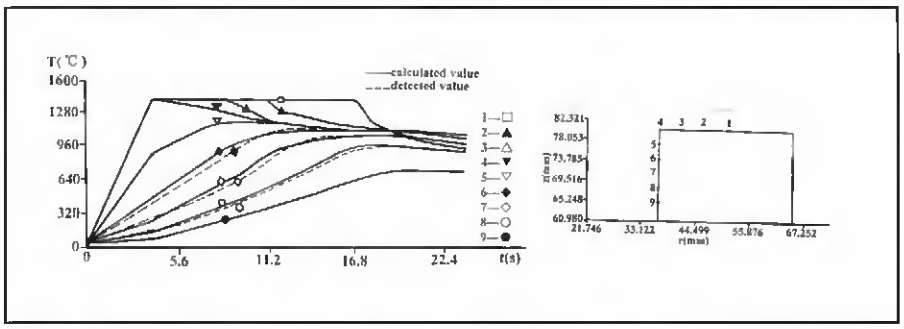

Fig. 3 — The comparison between the calculated value and detected value of the thermal circle curve on some measurable points of weld joints.

Table 2 — Mechanics Properties of the 36CrNiMo4 Steel

Temperature (K)	293	573	773	973	1173	1373	1573
Elastic modulus E (GPa)	200	183	148	148	148	148	148
Heat expansion efficiency α	11.37×10^{-6}	14.6×10^{-6}	14.7×10^{-6}	14.7×10^{-6}	14.7×10^{-6}	14.7×10^{-6}	14.7×10^{-6}
Poisson ratio μ	0.25	0.26	0.32	0.32	0.32	0.32	0.32
Flow stress σ_s(MPa)	1010	790	580	460	195	95	80

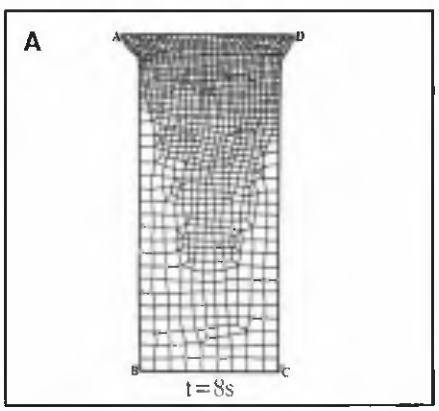

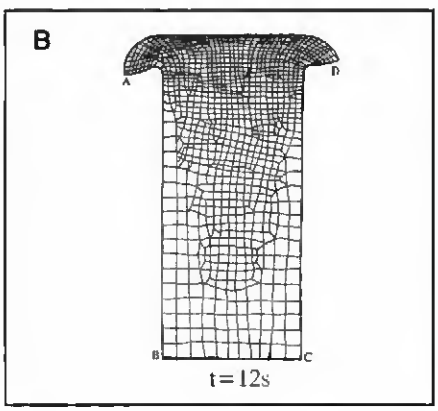

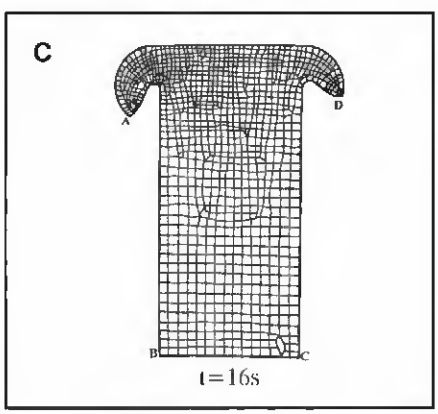

Fig. 4 — Variation of the gridding in a quarter section of the welded joint with time of welding. A — t = 8 s; B — t = 12 s; C — t = 16 s.

$$\left[C\right]\left\{\dot{T}\right\} + \left[K\right]\left\{T\right\} = \left\{Q\right\} \quad (9)$$

where $[C]$ is the entropy production rate matrix; $[K]$ is the heat transmission matrix; $\{Q\}$ is the general heat flow vector matrix.

$$\left(\left[K_0\right] + \left[K_s\right]\right)\left\{\dot{\alpha}\right\} = \left\{\dot{R}\right\} \quad (10)$$

where $[K_0]$ is the small deformation elastoplastic rigidity matrix; $[K_s]$ is the initial stress element rigidity matrix; $\{\dot{\alpha}\}$ is the speed strain vector of the panel point of matter; $\{\dot{R}\}$ is the load rate vector (including thermal load).

The experimental investigations were carried out on-site at BaoGang Inc., Shanghai. Oil drillers made of 36CrNiMo4

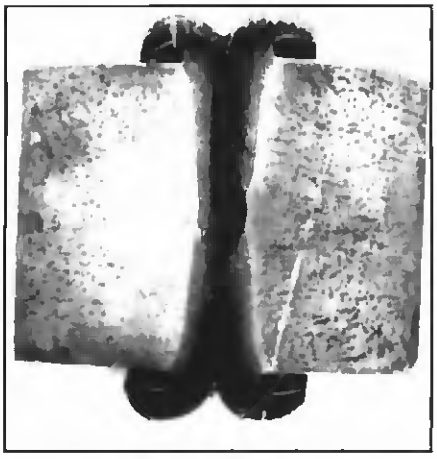

Fig. 5 — The macrostructure in the one-quarter section of the joint after welding (X1.2).

steel were welded on an inertia friction machine B320. The inner and outer radii of all specimens were 37 and 66.25 mm, respectively. The lengths of the welded specimens were 300 and 8000 mm, respectively. The parameters selected for the experiments were a rotating speed of 1050 rpm, a total mass moment of inertia at 220 lb-in.-s^2, and a constant thrust force throughout the welding cycle at 130 bar. The length used for calculations was 80 mm, because the heat- and force-affected zone (HFZ) of the friction welded joint is very short. In addition, a quarter section of the joint was used for the calculation because of the axial symmetry of the joint. The thermal and mechanical properties of the 36CrNiMo4 steel used for numerical analyses are listed in Tables 1 and 2, respectively.

Results and Discussions

Temperature Distribution

With the above-mentioned numerical model, temperature distributions during friction welding were numerically calculated. The calculated results are given in Figs. 2 and 3. Figure 2 shows isothermal distribution in a cross section of a quarter of the joint at 8, 12, and 16 seconds, respectively, during welding. Figure 3 illustrates temperature variation at nine positions of time for the weldment, which are indicated in the right side of the figure. As indicated in Figs. 2 and 3 (especially Fig. 3), the hot zone with the temperature above 800°C is about 8 mm near the weld line (frictional surface). Figure 3 also indicates the temperature near the weld line (frictional surface) was at its maximum at the very beginning (about 5 s) of friction welding. A very high heating rate and a steep temperature gradient were near the weld line (frictional surface). Moreover, the closer the position was to the weld line, the higher the temperature and the heating rate, as shown in Fig. 3.

The infrared detection method is used to measure the thermal cycle curve at the positions on the surface of the weldment, which are indicated in the right side of Fig. 3. The measured results are also plotted in Fig. 3 (left side) by dashed lines in order to compare them with those numerically calculated (solid lines). The measured curves are plotted from the means of five readings. They show a fit with the calculated results.

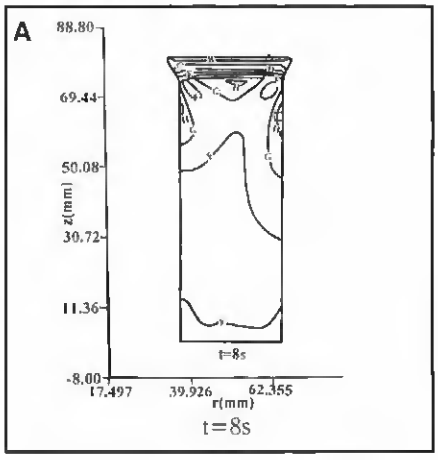

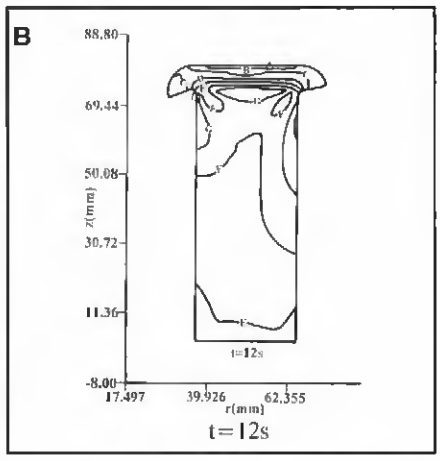

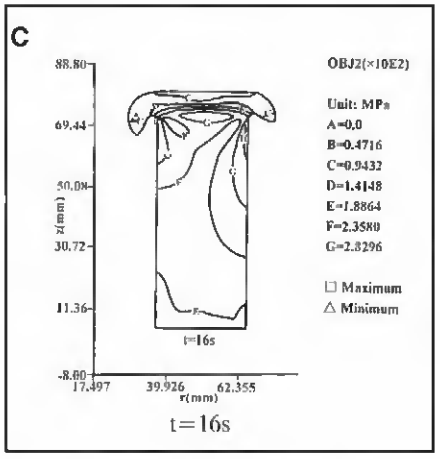

Fig. 6 — Variation of the equivalent stress distribution in a quarter section of the joint with time of welding. A — t = 8 s ; B — t = 12 s; C — t = 16 s.

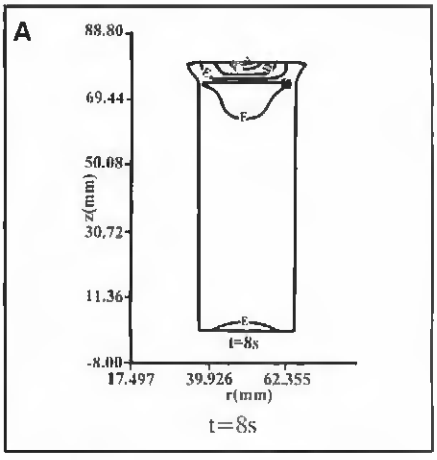

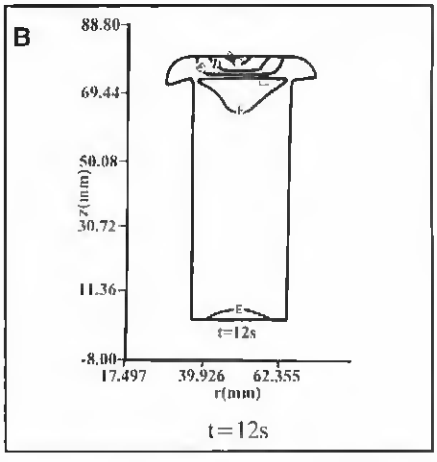

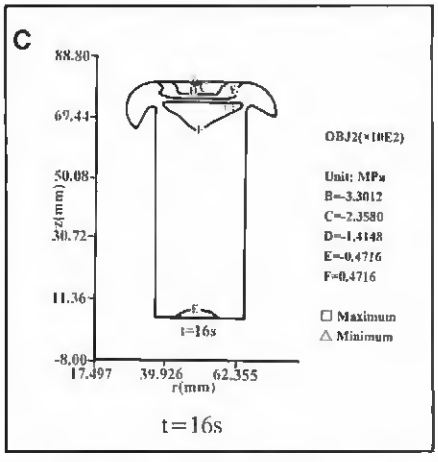

Fig. 7 — The radial stress distribution in a quarter section of the joint during welding. A — t = 8 s ; B — t = 12 s; C — t = 16 s.

Deformation

The calculated results for the deformation of the weldment (G zone as shown in Fig. 1) are shown in Fig. 4. The deforma-

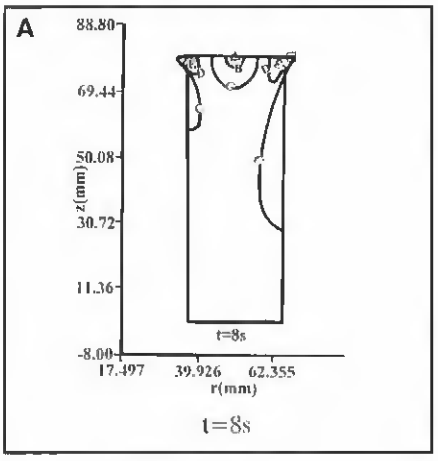

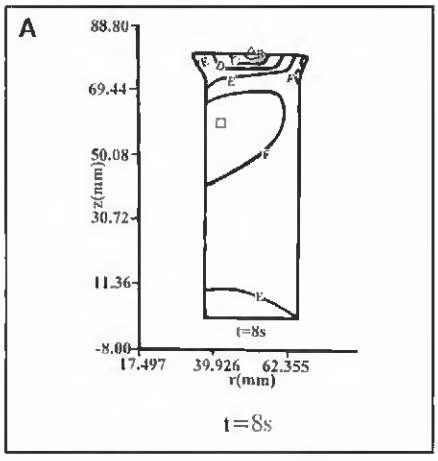

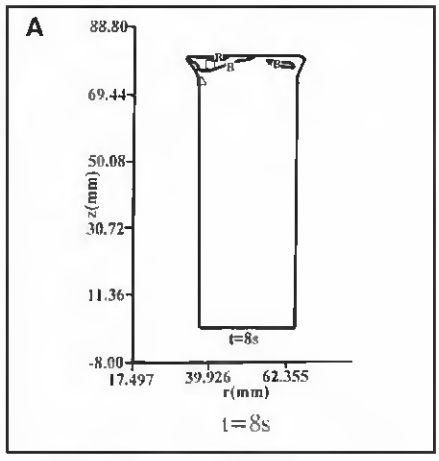

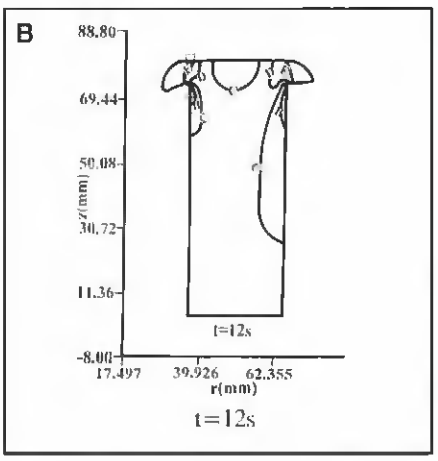

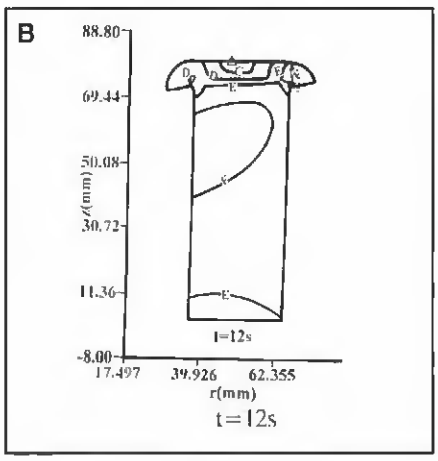

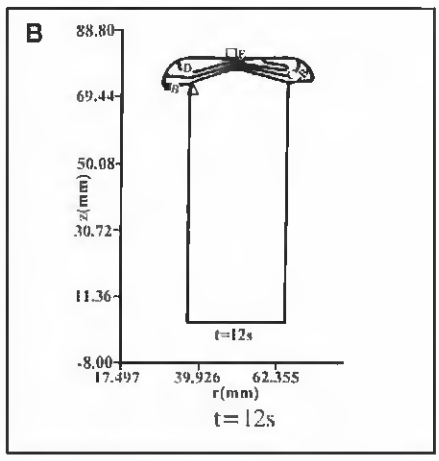

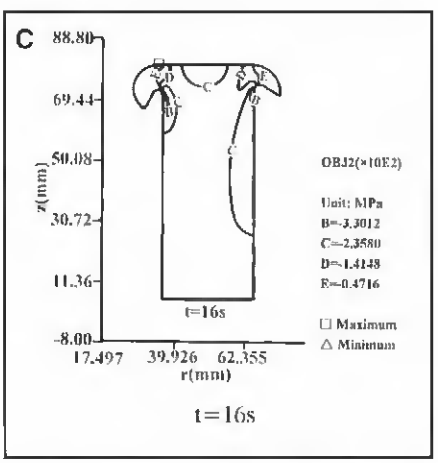

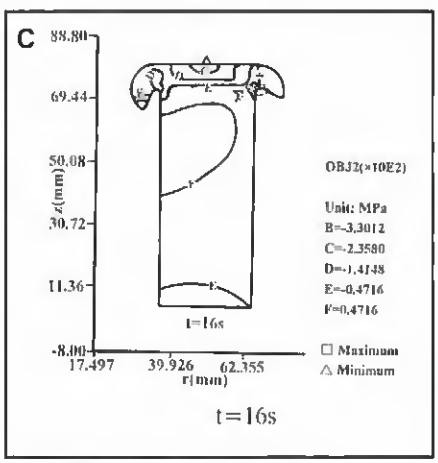

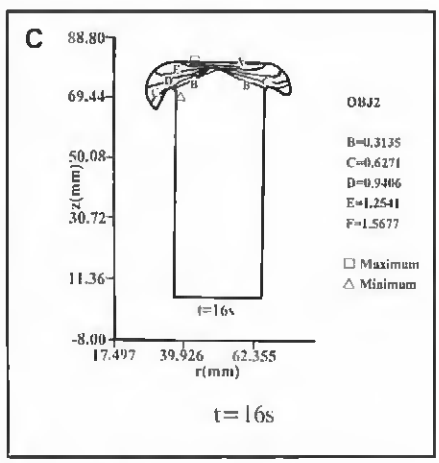

Fig.8 — The axial stress distribution in a quarter section of the joint during welding. A — t = 8 s; B — t = 12 s; C — t = 16 s.

Fig. 9 — The tangential stress distribution in a quarter section of the joint during welding. A — t = 8 s; B — t = 12 s; C — t = 16 s.

Fig. 10 — Variation of the equivalent strain distribution in a quarter section of the joint with time of welding. A — t = 8 s; B — t = 12 s; C — t = 16 s.

tion concentrates mainly near the frictional surface. The extruded shape gradually forms near the welded joint during the welding process. Figure 5 shows the longitudinal macrostructure in the one-quarter cross section of the welded joint. Comparing numerically calculated results in Fig. 4 with the experimental observations in Fig. 5, one can conclude an excellent fit between them. The extruded shape is asymmetric, as shown in Fig. 5. It results from nonuniform material properties along the radial direction of the specimen during welding, as the thermomechanical model predicts — Fig. 4C.

Stress

As shown in Fig. 6, the locations where the maximum and minimum of the equivalent stress appear vary with time during the welding process. At the late stage of inertia welding, the maximum existed near the inner circle at the reentrant part of the joint (the extruded shape).

The stress components in the one-quarter section of the joint during the welding process are shown in Figs. 7–9. The radial stress along the whole joint (the deformation zone near the weld line) is

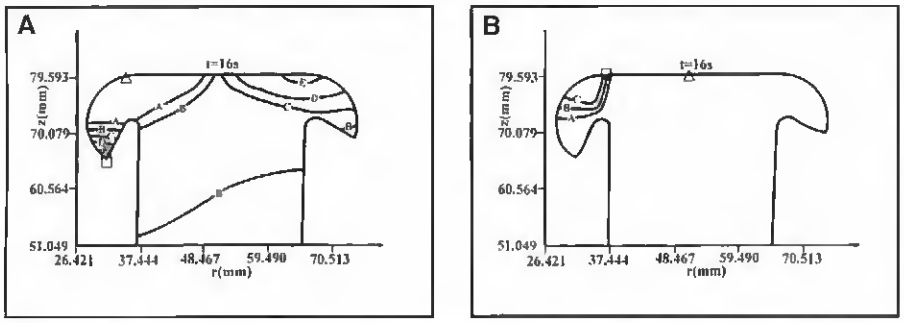

Fig. 11 — The strain rate component distribution in a quarter section of the joint at the end of welding. A — Tangential strain rate; B — radial strain rate.

compressive stress and reaches the maximum near the center of the frictional surface. However, because of the formation of the extruded shape near the welded joint, the radial stress becomes tensile stress between the deformation and nondeformation zones. The tensile stress values range between 145 and 160 MPa at different stages of welding.

The axial stress of the welded joint is all compressive stress, as shown in Fig. 8. The maximum is near the center of the welded joint. The stress values are smaller in the zone near the inner and outer circle of the welded pipe. The tangential stress appears as tensile stress at the root of the upset metal near the outer circle of the welded pipe, as shown in Fig. 9. Its value varies from 92 to 136 MPa during the welding process.

Strain and Strain Rate

Distribution of equivalent strain in one quarter of the joint during welding is shown in Fig. 10. The maximum appears near the middle zone of the pipe wall on the weld interface. In addition, the maximum at this zone arrived at 2.216 at the end of welding (16 s in this study).

Figure 11 indicates the tangential strain rate reaches maximum at the tip of the upset metal at the inner radius of the specimen (point A in Fig. 1) at the end of welding. The defect resulted from the large tangential strain rate maybe appearing at the tip of the upset metal at the inner radius of the specimen. The calculated results of the radial strain rate show its maximum occurs at the inner circle zone on the weld interface and the minimum in the center of the frictional surface at the end of welding.

Summary

Numerical calculations and experiments have been done to analyze the inertia friction welding process, which is a typical process with a high temperature, large deformation, and transient operation. The mathematical model of inertia welding has been presented. The coupled effects of the mechanics and heat transfer are taken into account in the model. The distributions of temperature, deformation, stress, strain, and strain rate during the inertia welding process were numerically analyzed. The simulation results of temperature were in good agreement with the experimental points. The calculated results of the deformation also fit excellently with those experimentally observed.

With the finite element method (FEM) numerical simulation used in this paper, distribution of welding temperature, flow stress, and plastic strain, as well as the variability regularity of the thermodynamic parameters, such as strain rate, can be obtained. That means this model can be used as an industrial tool to predict evolution of temperature, stress, strain, and final geometry of the welded parts.

In future work, the dynamic recrystallization grain size equation of the welded material can be gotten by means of isothermal and constant strain rate tests, and then combined with the grain size model and the FEM model in this paper to analyze and predict the microstructure and property of the welded joint. Meanwhile, by analyzing metal flow and distribution of stress and strain, the formation and development of a fracture near the weld zone can be predicted, which then can be used to optimize welding parameters.

References

1. Sluzalec, A. 1990. Thermal effects in friction welding. *Int. J. Mech. Sci.* 32(6): 467–478.

2. Wang, K. K. 1970. Transient temperature distribution in inertia welding of steels. *Welding Journal* 49(12): 419-s to 425-s.

3. Kozo, O. 1982. Effect of heat balance at interface on friction welding of equi-diameter bar joints (Japanese). *J. JWS* 51(2): 134–141.

4. Fu, L., and Duan, L. Y. 1998. The coupled deformation and heat flow analysis by finite element method during friction welding. *Welding Journal* 77(5): 202-s to 207-s.

5. Rich, T. 1971. The forge phase of friction welding. *Welding Journal* 50(3): 137-s to 146-s.

6. Wang, K. K. 1974. Flywheel friction welding research. *Welding Journal* 53(6): 233-s to 242-s.

7. Moal, A., and Massoni, E. 1995. Finite element simulation of the inertia welding of two similar parts. *Engineering Computations* 12(6): 497–512.

8. Moal, A., Massoni, E., and Chenot, J. L. 1992. A finite element modeling for the inertia welding process. *Proc. of Int. Conf. on Computational Plasticity*, Pineridge Press, Barcelona, 1: 289–300.